A general purpose 2D Schrödinger solver with open/closed boundary conditions for quantum device analysis

A. Abramo
INFM – Department of Physics, University of Modena, Italy

1997

***Abstract*— In this paper a two-dimensional Schrödinger simulator devised for the analysis of steady state coherent transport in electron devices is presented. The simulator provides the solution of the time-independent Schrödinger equation inside a generic two-dimensional system with closed- or open-boundary conditions. The solution is determined in presence of a generic potential energy profile and, optionally, of a constant magnetic field in the perpendicular direction. The program has been applied to the solution of simple two-dimensional problems, chosen as representative sketches of physical situations of practical interest.**

I. Introduction

Thanks to the constant progress of modern solid-state technologies, the continuous scaling of device dimensions has produced nowadays state-of-the-art MOS transistors, featuring channel lengths in the deep submicron range. In this length range, devices show substantial quantum effects, such as carrier confinement [1] and localized impurities [2]. As a consequence, the quantum mechanical treatment of the electron transport will be soon of practical interest. In addition, its relevance will certainly increase, especially in view of new device design concepts based on quantum wells, single electron, and tunneling effects [3], [4].

Due to recent improvements, the fully-quantum one-dimensional (1D) analysis of carrier transport is almost within everyone's grasp [5], but it still remains a formidable task, owing both to the complexity of the physics and to the heavy computational burden involved. Simpler or partial alternatives to quantum transport have been investigated, and so far 1D approaches [6]–[8] or two-dimensional (2D) corrections [9] to somehow include the effects of quantum phenomena inside a device simulator have been proposed.

In this paper a 2D Schrödinger simulator devised for the analysis of steady-state, coherent transport in electron devices is presented. The simulator provides the solution of the time-independent Schrödinger equation inside a generic 2D system with closed- (CBC) or open-boundary (OBC) conditions, in presence of a generic potential energy profile ($E(\vec{r})$) and, optionally, of a constant perpendicular magnetic field ($B_{\perp}$).

A. Abramo is currently with DIEGM, University of Udine, via delle Scienze, 208, I-33100, Udine (Italy) phone.: +39-432-558283, fax. +39-432-558251, e.mail.: abramo@picolit.diegm.uniud.it.

This work was supported by A.R.O, O.N.R, and E.R.O., all gratefully acknowledged.

II. The simulator

The simulator computes for the solution inside a 2D system which, in our notation, is a generic 2D space region (see Fig. 1) everywhere isolated from the outside by Dirichlet (i.e. $\Psi = 0$) CBCs but at the optional interfaces between the system and its leads. These are quantum wells of constant sections through which the system exchanges charge with the reservoirs. The leads are connected to the system by OBCs which are the superposition of progressive and regressive plane waves and evanescent modes (we follow [10], [11] for the OBCs form and for the notation):

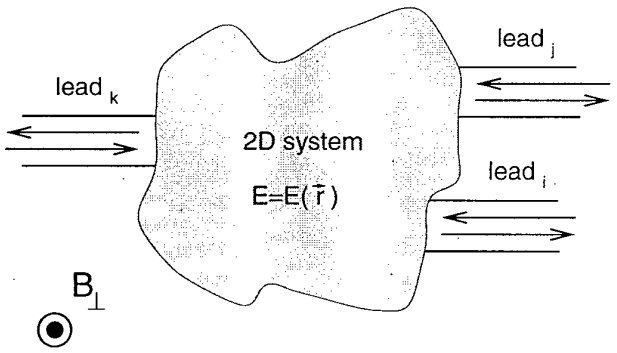

Fig. 1. A sketch of the generic 2D system. The system leads are optional. In their absence the system is closed.

$$\Psi_j(\eta_j,\xi_j) = \sum_{m=1}^{N^j}\left[a_m^j\chi_m^j(\xi_j)e^{-ik_m^j\eta_j} + b_m^j\chi_m^j(\xi_j)e^{ik_m^j\eta_j}\right] + \\ + \sum_{m=N^j+1}^{\infty} b_m^j\chi_m^j(\xi_j)e^{-k_m^j\eta_j} \qquad (1)$$

where: j is the index of the lead; η_j and ξ_j are the longitudinal-outgoing and counter-clockwise transverse coordinate of lead j, respectively; m is the index of the transverse modes inside the leads: N^j is the number of traveling modes inside lead j; k_m^j is the wave vector of the m^{th} mode inside lead j; a_m^j and b_m^j are the strengths

of the incoming and reflected m^{th} mode in lead j, respectively; finally,

$$\chi_m^j(\xi_j) = \sqrt{\frac{2}{d_j}} sin\left[\frac{m\pi}{d_j}\right] \tag{2}$$

is the m^{th} transverse mode of the wave function inside lead j of width d_j.

For sake of flexibility, the program reads a triangular mesh describing the generic 2D domain to be simulated, together with its 2D $E(\vec{r})$ [12]. The 2D envelope-function equation (i.e. the time-independent Schrödinger equation in the effective mass approximation) is then discretized in the *finite elements* framework, leading to the following linear system of equations ($B_\perp = 0$ in this case) [10], [11]:

$$\sum_{j=1}^{N}\left[\left(\frac{\hbar^2}{2m^*}\int_\Omega \nabla\varphi_i\cdot\nabla\varphi_j\,d\Omega + \int_\Omega E(\vec{r})\,\varphi_i\,\varphi_j\,d\Omega\right) - \right.$$

$$\left. - \epsilon^{(m)}\int_\Omega \varphi_i\,\varphi_j\,d\Omega\right]\Psi_j^{(m)} =$$

$$= \frac{\hbar^2}{2m^*}\int_\Gamma\left(\varphi_i\,\nabla\Psi^{(m)}\right)\cdot\hat{n}\,d\Gamma \tag{3}$$

where: $i = 1...N$ are the mesh nodes; m^* is the carrier effective mass; $\Psi_j^{(m)}$ is the unknown eigenfunction value relative to the m-th eigenvalue $\epsilon^{(m)}$ at node j; Ω is the 2D domain of integration; Γ are the system boundaries; $\varphi_k(\vec{r})$ are the so called *shape* (or *basis*) *functions* which impose the functional nature of the solution. Since we chose to linearly approximate the $\Psi^{(m)}$ in each triangular element, $\varphi_k(\vec{r})$ is the plane being unity at node k and zero at the other two nodes of the element.

If $B_\perp \neq 0$ the system (3) becomes more complex because the OBCs are not known *a priori* and must be previously determined solving a non-linear, non-symmetric generalized eigenvalue problem.

The symmetric generalized eigenvalue problem (3) is assembled in sparse form and then solved. The solution is found by means of the *inverse iteration* and *Rayleigh quotient* algorithms, where the minimum of the potential energy is used as a guess of the lowest energy eigenvalue. Successive eigenfunctions and eigenvalues are obtained starting from an eigenfunction guess orthonormal (through Gram-Schmidt procedure) to all previous ones, and using the last eigenvalue as a guess for the successive. The determination of each eigenstate requires the inversion of symmetric, positive-definite matrices. This task is carried out using a Preconditioned Conjugate Gradient (PCG) algorithm. In addition, $B_\perp \neq 0$ requires the use of a bilinear-PCG algorithm for the determination of the OBCs.

III. Simulation results

The program has been applied to the simulation of 2D test systems. Despite to its simple nature, each example should be viewed as the attempt to investigate quantum effects present inside real mesoscopic devices. Since the final goal will be the coherent simulation of a submicron MOS transistor, the reader is allowed to catch the flavor of it in each of the shown examples.

The feature length of modern MOSFET devices is becoming so short that the assumption of a uniform background doping of the channel region is no longer realistic [2], [13]. In a quantum simulation the role of localized Coulomb impurity can be included directly inside the potential term $E(\vec{r})$. Fig. 2 shows $|\Psi|^2$ inside a rectangular OBC resonant cavity with (right) and without (left) the presence of an unscreened Coulomb impurity in its central position. The stopping effect on the eigenfunction propagation from $x = 0$Å to $x = 100$Å due to the repulsive impurity is clearly seen, and some tunneling of the wave function can be observed.

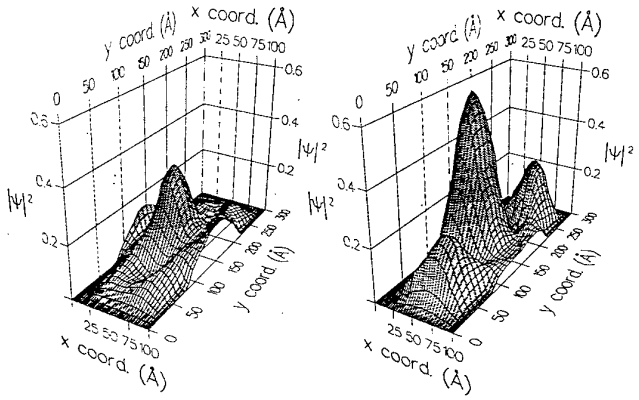

Fig. 2. $|\Psi|^2$ inside a OBC rectangular cavity with (right) and without (left) a repulsive Coulomb potential in its central position. OBCs at the extreme x sections and for 100Å $\leq y \leq$ 200Å; CBCs elsewhere. The Coulomb impurity reduces propagation along x.

The role of the roughness of the $Si - SiO_2$ interface on the degradation of carrier mobility has been widely investigated [6], [14], [15]. Again, this is a typical feature that can be directly included inside the quantum simulation of carrier transport. Fig. 3 shows the localization of the eigenfunctions inside quantum wells of different lengths featuring a Gaussian roughness on one of the interfaces, schematically representing the $Si - SiO_2$ interface of a quantized MOS channel. As the channel length is increased, the localization effect increases. Therefore, the channel conductance $\sigma(\epsilon)$ is progressively reduced, as shown in Fig. 4 where $\sigma(\epsilon)$ for two of the rough channels of Fig. 3 (broken lines) are reported, together with the conductance of a channel with ideal $Si - SiO_2$ interface. Here, $\sigma(\epsilon)$ has been obtained summing up the conductances of all transverse modes present at energy ϵ. As can be seen, the detrimental effect of surface roughness increases with increasing channel length, driving $\sigma(\epsilon)$ away from the stepwise behavior typical of quantized channels featuring ideal interfaces.

Fig. 5 shows $|\Psi|^2$ inside a quantum well of increasing width, as can be schematically regarded the channel of

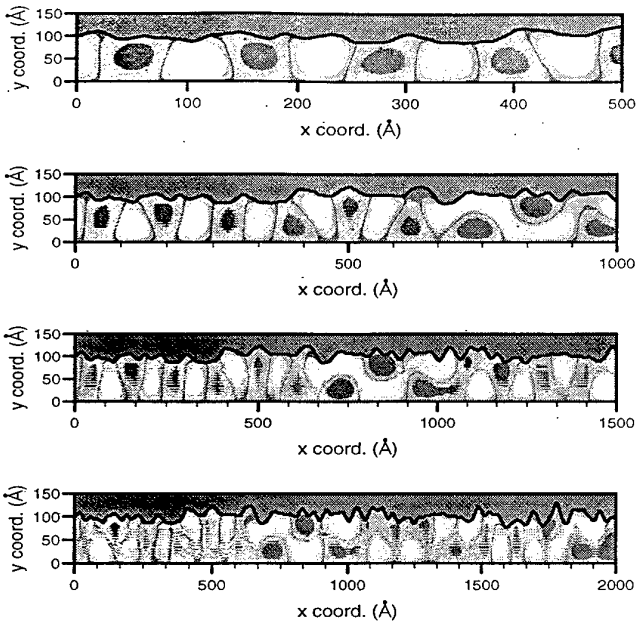

Fig. 3. $\mathcal{R}e[\Psi]$ inside few schematic OBC MOS rough channels of different lengths. Gray shade: $E(\vec{r}) = 3.15V$ (i.e. SiO_2); $E(\vec{r}) = 0V$ elsewhere. OBCs at the extreme x sections; CBCs elsewhere. Localization increases (thus conductance decreases) with increasing channel length.

a MOS transistor, whose transverse section widens moving from source to drain under the effect of the applied V_{DS} (although, for simplicity, we assumed no potential drop along the channel). Since each solution represents an eigenstate relative to a specific value of the total energy ϵ, the last divides in some way (the problem is not separable) between its longitudinal and transverse components. However, wider sections of the channel imply lower transverse energy. Thus, a momentum (or energy) transfer from the transverse to the longitudinal direction is expected as long as the channel width increases. This effect can bee seen from the *waterfall*-like shape of the solution.

The solver can also be applied to physical situations closer to what is the common understanding of the term *mesoscopic*. Fig. 6 shows the $|\Psi|^2$ inside an OBC quantum well in presence of a biconcave $E(\vec{r})$ (solid line; see Figure Caption) [16], [17]. The focusing effect of the electron beam is clearly seen. Looking at the arrows, representing the carrier quantum current, it is clear how the focusing effects does not simply originate from carriers tunneling through the barrier at the thinnest sections, but from the converging effect on the electron wave of the shaped potential, even at barrier points where sections are larger (see explanations in [16], [17]).

Finally, as a simple example of a solution including the presence of a non-zero perpendicular magnetic field, Fig. 7 shows the coherent transport through a quantized channel in presence of $B_\perp = 25T$. As can be seen, the wave function, entering from the left OBC, proceeds towards the right OBC displaced towards the upper edge due to the presence of the constant $B_\perp$.

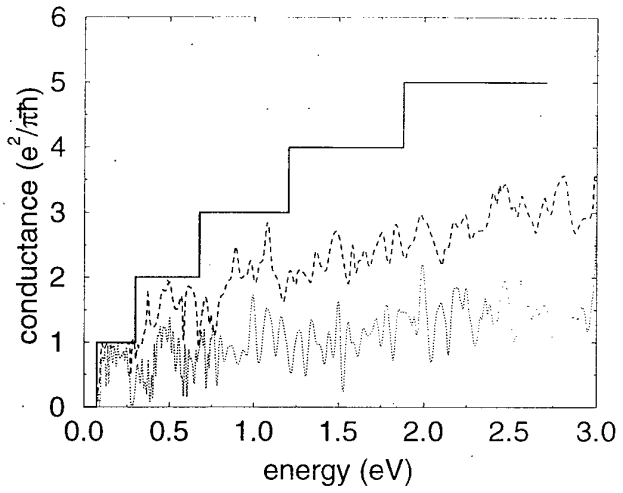

Fig. 4. Conductance of two of the rough channels Fig. 3: dashed line: 500Å channel; dotted line: 2000Å channel; solid line: conductance of an ideal channel of the same width.

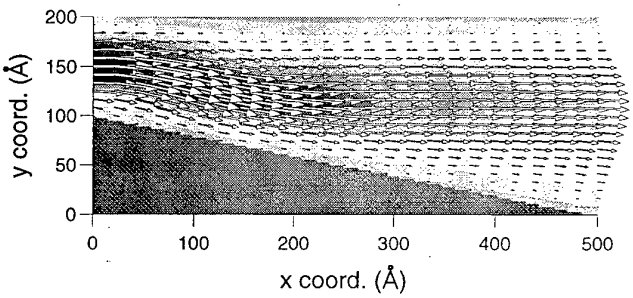

Fig. 5. $|\Psi|^2$ inside a OBC quantum well of linearly increasing section. Gray shade: $E(\vec{r}) = 3V$; $E(\vec{r}) = 0V$ elsewhere. Arrows: quantum current flux. OBCs at the extreme x sections; CBCs elsewhere. The energy transfer between the transverse and the longitudinal direction is seen.

IV. Conclusions

A 2D Schrödinger simulator devised for the analysis of steady-state, coherent transport in electron devices has been developed. The simulator, providing the solution of the time-independent Schrödinger equation inside a generic 2D systems, can be usefully employed for the analysis of quantum coherent transport in mesoscopic devices. Results of simple but potentially relevant applications have been shown, encouraging the use of such approach to the analysis, only coherent for the moment, of submicron devices.

Acknowledgment

The author is indebted to Prof. C. Jacoboni and Dr. P. Casarini for the many helpful discussions.

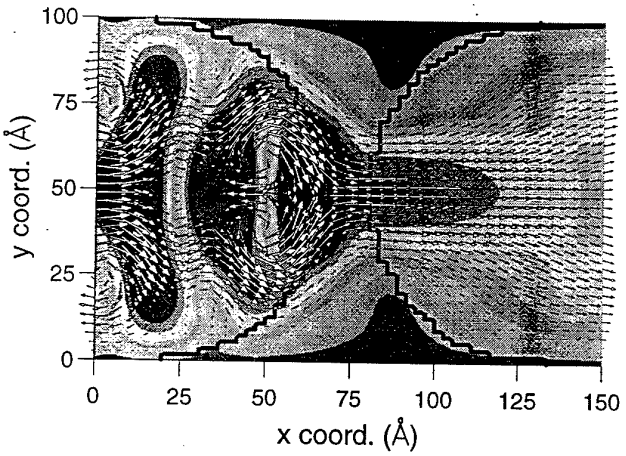

Fig. 6. $|\Psi|^2$ of an OBC focusing electronic lens. Solid line: edge contour of a biconcave shaped potential ($E(\vec{r}) = 0.25V$ therein) realizing the electrostatic lens. Arrows: quantum current flux. OBCs at the extreme x sections; CBCs elsewhere.

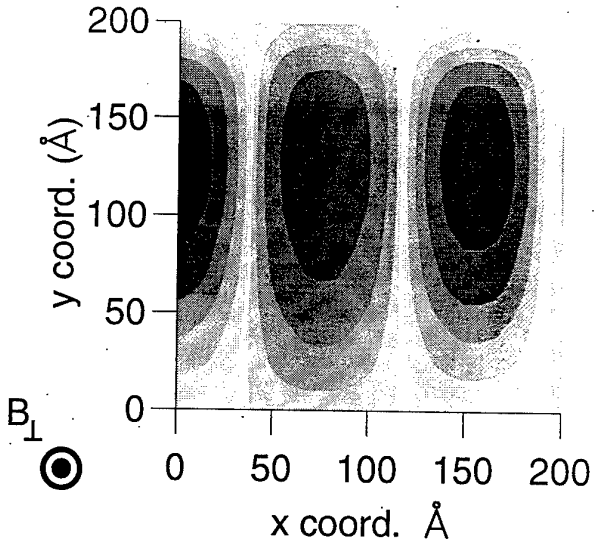

Fig. 7. $\mathcal{R}e[\Psi]$ inside an OBC quantum well with $E(\vec{r}) = 0V$ inside but in presence of a constant $B_\perp$, displacing $\mathcal{R}e[\Psi]$ towards the upper edge. OBCs at the extreme x sections; CBCs elsewhere. $B_\perp = 25T$.

REFERENCES

[1] S. Takagi and A. Toriumi, "Quantitative understanding of inversion-layer capacitance in Si MOSFET's", *IEEE Trans. Electron Devices*, vol. 42, pp. 2125–2130, 1995.

[2] H-S. Wong and Y. Taur, "Atomistic simulation of discrete random dopant distribution effect in sub-0.1μm MOSFET's", in *IEDM Tech. Dig.*, 1993, pp. 705–707.

[3] A. Nakajima, T. Futatsugi, K. Kosemura, T. Fukano, and N. Yokoyama, "Room temperature operation of Si single-electron memory with self-aligned floating dot gate", in *IEDM Tech. Dig.*, 1996, pp. 952–954.

[4] L. Guo, E. Leobandung, and S.Y. Chou, "Si single-electron MOS memory with nanoscale floating-gate and narrow channel", in *IEDM Tech. Dig.*, 1996, pp. 955–956.

[5] C. Jacoboni, A. Abramo, P. Bordone, R. Brunetti, and M. Pascoli, "Application of the Wigner-function formulation to mesoscopic systems in presence of electron-phonon interaction", in *Proc. of the Int. Workshop on Computational Electronics*, 1997 (to be published).

[6] T. Ando, A.B. Fowler, and F. Stern, "Electronic properties of two-dimensional systems", *Rev. Mod. Phys.*, vol. 54, pp. 437–672, 1982.

[7] S. Jallepalli, J. Bude, W.-K. Shih, M.R. Pinto, C.M. Maziar, and Jr. A.F. Tasch, "Electron and hole quantization and their impact on deep submicron p- and n-MOSFET characteristics", *IEEE Trans. Electron Devices*, vol. 44, pp. 297–303, 1997.

[8] K.S. Krisch, J.D. Bude, and L. Manchanda, "Gate capacitance attenuation in MOS devices with thin gate dielectrics", *IEEE Electron Device Lett.*, vol. 11, pp. 521–524, 1997.

[9] A. Spinelli, A. Benvenuti, and A. Pacelli, "Investigation of quantum effects in highly doped MOSFETs by means of a self-consistent 2D model", in *IEDM Tech. Dig.*, 1996, pp. 399–402.

[10] C. Lent and D.J. Kirkner, "The quantum trasmitting boundary method", *J. Appl. Phys.*, vol. 67, pp. 6353–6359, 1990.

[11] M. Leng and C.S. Lent, "Quantum transmitting boundary method in a magnetic field", *J. Appl. Phys.*, vol. 76, pp. 2240–2248, 1994.

[12] M.R. Pinto, C.S. Rafferty, and R.W. Dutton, "PISCES-II: Poisson and continuity equation solver", Tech. Rep., Stanford Electronics Labs, 1984.

[13] J.R. Zhou and D.K. Ferry, "Three-dimensional simulation of the effect of random impurity distribution on conductance for deep submicron devices", in *Proc. of the Int. Workshop on Computational Electronics*, 1994, pp. 74–77.

[14] S.M. Goodnick, D.K. Ferry, C.W. Wilmsen, Z. Lilental, D. Fathy, and O.L. Krivanek, "Surface roughness at the $Si(100) - SiO_2$ interface", *Phys. Rev. B*, vol. 32, pp. 8171–8186, 1985.

[15] M.V. Fischetti and S. Laux, "Monte Carlo study of electron transport in silicon inversion layers", *Phys. Rev. B*, vol. 48, pp. 2244–2274, 1993.

[16] J. Spector, H.L. Stormer, K.W. Baldwin, L.N. Pfeiffer, and K.W. Wast, "Electron focusing in two-dimensional systems by mean of an electrostatic lens", *Appl. Phys. Lett.*, vol. 56, pp. 1290–1292, 1990.

[17] U. Sivan, M. Heiblum, C.P. Umbach, and H. Shtrikman, "Electrostatic electron lens in the ballistic regime", *Phys. Rev. B*, vol. 41, pp. 7937–7940, 1990.